A Finite Element Approach to Conduct Machinability Studies on Age-Hardened AA6061 Matrix Hybrid Composites

Anand Pai, Laxmikant G Keni & Chandrakant R Kini[*]

Department of Aeronautical and Automobile Engineering, Manipal Institute of Technology, Manipal Academy of Higher Education, Manipal-576104, India
*Email: chandra.kini@manipal.edu

Highlights:

- AA6061-T6 matrix composites with graphite and granite dust fillers were synthesized by stir casting.
- Mechanical characterization was carried out and the properties for the finite element analysis were noted.
- A peripheral milling cutter was designed with the commercial software ANSYS and the LS-DYNA module was used to study the response of the materials to machining.

Abstract. AA6061, a popular structural material, has found widespread usage in the automotive and aerospace domains. The current work explored the effect of the improvement of mechanical properties on the machinability of AA6061 through finite element analysis. Three compositions of AA6061 containing 2 wt.% graphite and 0, 2, 4 wt.% granite dust were fabricated by stir casting. In the current work, a finite element model of a slab milling cutter with eight teeth was designed with high-speed steel (HSS) as the tool material. The LS-DYNA module of ANSYS was used for simulation of the milling operation, selecting two peripheral speeds for the cutter during the machining of the workpiece. Surface milling was carried out on the cast slabs of the three compositions to study chip formation. At higher cutting speeds, there was an increase in the von Mises stress as well as material deformation. An increase in the weight fraction of the ceramic fillers led to a corresponding increase in the von Mises stress and material deformation. The experimental results from face milling of the three compositions showed that the surface roughness increased with an increase in the content of ceramic fillers and a decrease in chip size.

1 Introduction

The usage of high-performing metal matrix-fiber composites in aerospace, civil engineering, defence and automotive applications has been gaining extreme prominence over the past few decades. After iron, aluminum is the most highly

used metal. Due to its excellent formability, low density, high toughness, good thermal conductivity and corrosion resistance, it is an excellent matrix material. Aluminum alloys are manufactured by adding Mg, Si, Cu and other metals with densities close to pure aluminum, 2700-2800 kg/m^3. The melting point of aluminum is close to 700 °C due to which it can be easily processed by solid-state routes (such as powder metallurgy and in-situ techniques) and by liquid casting methods. Table 1 compares the mechanical properties of different materials [1]. In structural materials like aluminum alloys, continuing advancements range from increasing the specific strength, toughness, corrosion resistance to developing light-weight aluminum matrix composites (AMC) with low-cost implications [2]. Adding reinforcements that are harder and stronger tend to improve the properties of the combined materials [3].

Several reinforcements have been considered in recent work to improve the mechanical response of aluminum alloys. Graphite as a dry lubricant is used for reinforcing aluminum alloys owing to its high lubricity, chemical inertness, non-abrasive nature, film-forming capability on metal surfaces and eco-friendliness. The addition of graphite particulates decelerates the wear of AMCs in operation but alters the strength of AMCs with a reduction in flexural strength and hardness [3]. Therefore, ceramic particles as reinforcements in addition to graphite serve the purpose of augmenting the mechanical performance. Some of the widely used reinforcements for aluminum matrix composites like SiC, B$_4$C, Al$_2$O$_3$, and fly ash are known to provide considerable enhancement to the mechanical properties of hardness and strength in AMCs. Hybrid AMCs are gaining prominence as structural materials. Deaquino-Lara *et al.* [4] used graphite of average particle size 21 μm and 0 to 1.5 wt.% for AA 7075 alloy. Continuous M40 J graphite fiber (Gr$_f$) of ~5 μm in diameter was used by Su *et al.* [5] with AA 6061 powders in 65 vol.% for pressure infiltration. Suresha *et al.* [6] used SiC in sizes 10-20 μm with fractions of 2.5% to 10% by weight along with graphite for LM 25 alloy in fatigue studies; Guo, *et al.* [7] used SiC of average particle size 45 μm in 10 vol.% for AA6061 alloy.

Chu, *et al.* [8] utilized SiC (~5 μm diameter) in tandem with coated and uncoated graphite fillers. Alidokht, *et al.* [9] employed SiC (~30 μm) and MoS$_2$ (5 μm) particulates for AA356 aluminum alloy fabrication by powder metallurgy. Baradeswaran, *et al.* [10] used boron carbide particulates for AA 6061 and AA 7075 hybrid composites along with B$_4$C at 10 wt.% and graphite at 5 wt.% with average particle size 16-20 μm. Poovazhagan, *et al.* [11] manufactured hybrid nanocomposites using AA6061 reinforced with different hybrid ratios of SiC (0.5, 1.0 and 1.5 vol.%) and B$_4$C (fixed 0.5 vol.%) nanoparticles. Narayanasamy, *et al.* [2] fabricated and studied the characteristics of AA6061 / TiO$_{2p}$ / Al$_2$O$_{3p}$ composites with 4 vol.% of TiO$_2$ and 8 vol.% of Al$_2$O$_3$. Alaneme, *et al.* [12] added rice husk ash (RHA) and alumina to Al-Mg-Si alloy. Ahamed, *et al.* [13] used

nano-sized Al_2O_3 and Y_2O_3 (particle size ~38 nm) particulates into monolithic AA6063 alloy matrix. Rajan, *et al.* [14] used fly ash with Al–7Si–0.35Mg alloy (356 cast Al alloy) for fabrication via stir casting route. The fly ash size was ~13 μm (5 and 10 wt.%). Murthy, *et al.* [15] used fly ash particles (size ~23 nm) in an AA 2024 matrix in 1-3 wt.% to fabricate Al–fly ash nanocomposites. Sudarshan, *et al.* [16] used fly ash for the study of aluminum alloy (A356) composites with two volume fractions (6 and 12 vol.%). Figure 1 shows the different routes employed for improving the mechanical properties of aluminum alloys and the need for machinability studies.
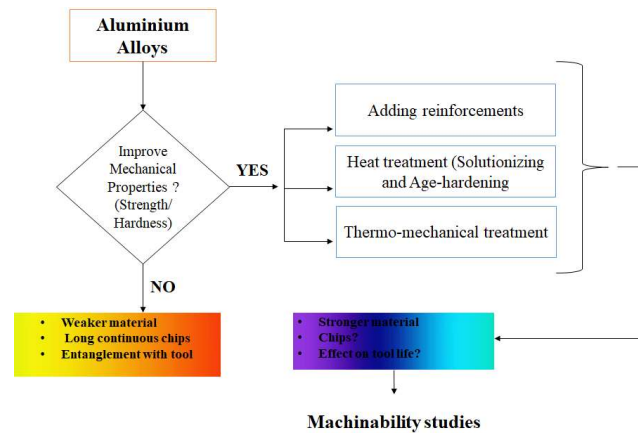

Figure 1 Effect of enhancement of the mechanical properties on machinability.

There have been simultaneous efforts to improve the mechanical response of aluminum alloys through thermal and thermo-mechanical treatment. Ozturk, *et al.* [17] carried out artificial ageing of commercially available AA 6061 alloy and studied the effect of ageing time on mechanical properties. Rajan, *et al.* [14] fabricated AA356 alloy composites with 5-15% fly ash by weight. The thermal treatment of T6 temper consisting of solutionizing (810 ± 10 K for 12 h), quenching in hot water (355 K) and then ageing (440 ± 10 K for 8 h) was carried out. There was an agglomeration of particles and high porosity in composites containing untreated fly ash. Adesola, *et al.* [18] investigated AA 6061 alloys for different temper treatments. The T4 temper consisted of solutionizing (813 K for 2 h), water quenching, and room temperature ageing for two weeks. The T8 temper consisted of thermomechanical treatment. The solutionizing treatment was carried out at 540 °C for 2 h, quenching in cold water followed by cold work up to 17%. Finally, ageing at 160 °C for 18 h was done. A time gap of 48 h between the solutionizing and ageing treatments was provided for grain refinement. Rajasekaran, *et al.* [19] compared the natural and artificial ageing

behavior of AA6061 composites containing SiC particulates. The T6 temper involved solutionizing treatment at 558 °C for 1 h. The ageing curves at different temperatures (room temperature up to 250 ºC) were plotted to determine the best ageing temperature. Pai *et al.* [20] and Sharma ,*et al.* [21] fabricated hybrid AA6061 matrix composites with graphite particulates and granite dust fillers. Ageing at 100°C was carried out to optimize the mechanical response.

Table 1   Comparison of mechanical properties of different materials [1].

Metal/ Alloys	Density, ρ (kg/m³)	Elasticity Modulus, E (MPa)	Tensile Strength σ_{ult} (MPa)	Coefficient of thermal expansion (°C⁻¹)	Useful Temperature Limit T_{max} (°C)
Steels	7800	205000	400-1600	1.3×10^{-5}	800
Aluminum alloys	2800	75000	450	2.2×10^{-5}	350
Titanium alloys	4400	105000	1200	0.8×10^{-5}	700
Copper	8800	125000	200-500	1.7×10^{-5}	650
Nickel	8900	220000	500-850	1.4×10^{-5}	900
Beryllium	1840	294000	200	1.2×10^{-5}	900
Silicon	2200	95000	--	--	1300

To cater to industrial applications like automotive and aerospace parts, the cast components may need to undergo various machining operations to obtain the desired shape and size suiting the design specifications. Enhanced mechanical properties offer many challenges in the machining of such heat-treated, hybrid ceramic reinforced aluminum alloy composites. Selection of the tool material, speed of cutting, depth of cut, and feed affect the surface quality, cutting force and cutting temperatures [22]. Finite element modeling is a popular approach for analyzing the machinability of different metals, alloys, composites and fiber/metal laminates [23-25]. Mebrahitom, *et al.* [26] used the finite element method to predict the cutting forces during side milling of AA6010 alloy using a two-fluted HSS flat end mill. A 3D orthogonal model was developed based on the ALE formulation. Spindle speeds of 18,336 and 21,392 rpm and a depth of cut of 2 mm were considered. In the experimental studies, a three-component force measurement dynamometer was employed during the end milling to record the cutting force. Krajinović, *et al.* [27] conducted simulation studies of the response of 42CrMo4 to milling operation with coated and uncoated tools. A 2D orthogonal cutting model using the arbitrary Lagrangian-Eulerian formulation was used for a simulation at 560 rpm. The base tool was a fine-grained hard metal tool with 3 wt.% Co. The materials used for coating the tools were TiAlN, TiCN/α-Al₂O₃ and TiAlN/α-Al₂O₃. The key metrics considered for the study were cutting force, tool-workpiece contact length, von Mises stress, tool surface temperature, and accumulated equivalent plastic strain. The authors concluded

that coating type had little or no effect on the von Mises stress, cutting force, and contact length. Yang, *et al.* [28] simulated the peripheral milling of Ti-6Al-4V alloy and analyzed the effect of feed rate and cutting speed on surface residual stress, compressive peak stress, and response depth. The authors conveyed that conversion of 3D peripheral milling (four-flute tool) to 2D orthogonal cutting saves computation time and effort without sacrificing accuracy. Johnson's constitutive model was used for the work material, along with the thermo-mechanical properties for the work and Tungsten carbide as the tool material. The authors developed a hybrid model using FEM and statistical models incorporating an exponentially damped cosine function, which showed good agreement with the experimental results.

The cutting speed and feed rate led to the conversion of residual stress from compressive to tensile, while causing a rise in the response depth. Davoudinejad, *et al.* [29,30] presented a 3D finite element model of slot micro end milling and contour up milling of AA6082-T6 alloy based on a Lagrangian finite element formulation for the coupled thermo-mechanical transient analysis. The actual tool geometry was implemented in the FE model. The key parameters – 3D chip flow shape, burr formation, and cutting forces – were studied and compared with the experimental data for milling carried out on a micro-milling center. The Johnson-Cook constitutive equation was used for AA6082-T6 alloy. Ucun, *et al.* [31] conducted finite element analysis of micro milling of Inconel 718 alloy, using uncoated tools, at four feed rates and a constant cutting speed of 48 m/min. The parameters of cutting force, tool stress, and cutting temperatures were measured. The authors reported that the feed rate directly affected these parameters.

From the literature it can be summarized that introducing ceramic and graphite reinforcements within aluminum alloys augments the mechanical properties hardness and strength. The properties can further be enhanced with an artificial ageing treatment consisting of solutionizing at 550 ºC followed by age-hardening. However, there is a need for predicting the machining response of ceramic and graphite-reinforced metal matrix composites to milling operations. In the current work, the fabrication of AA6061 with graphite and granite dust was carried out with the testing of mechanical properties and determination of the best ageing temperature. For conducting the machinability studies using finite element modeling, a 2D orthogonal cutting model was employed, and experimental studies for peripheral milling of fabricated compositions were carried out on a vertical machining center, followed by inspection of surface roughness, chip morphology, and surface texture studies using optical microscopy.

2 Methodology

Three compositions of AA 6061 hybrid composite were fabricated (reinforced with graphite particulates and crusher dust particulates) using the liquid stir casting method. The casting setup is shown in Figure 3(a), where AA6061 round billets were melted with the furnace temperature maintained at 850 °C. A stirrer speed of 450 rpm was used to create a vortex in the melt and pre-heated particulates of graphite and granite dust were added through a feed hopper with weight fractions based on the composition. Upon completion, degassing of the melt was carried out to dispel any dissolved gases and vapors, the melt was poured into the preheated molds shown in Figure 3(a). After cooling, the flat billets were cut to size for mechanical characterization and milling studies. Table 2 shows the details of the three compositions, with the corresponding nomenclature 2G, 2G2S and 2G4S. Solutionizing treatment was given at 550 °C. Artificial ageing was conducted at 100 °C and 180 °C to improve the mechanical properties. Tensile tests were conducted to evaluate the yield strength, tensile strength, and tangent modulus. Density measurements were conducted for the three compositions.

Table 2   Details of the three compositions considered.

Composition	Weight Percentage (%)		
	2G	2G2S	2G4S
Graphite	2	2	2
Granite Dust	-	2	4
AA6061	98	96	94

An eight-fluted slab milling cutter made of high-speed steel (HSS) was considered for carrying out the 2D orthogonal machining simulation utilizing ANSYS LS-DYNA. Figure 2 shows the 2D geometry of the milling cutter and the workpiece. The mechanical properties assigned to the workpiece in the model were taken for the work (see Table 3).
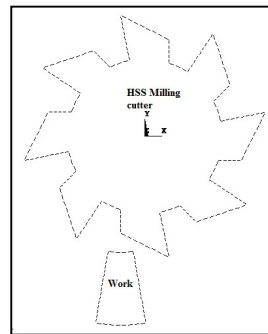

Figure 2   Slab milling cutter and workpiece.

The properties of the tool materials are shown in Table 4. A pitch circle diameter (PCD) of 60 mm was utilized for the milling cutter. The feed for aluminum and its alloys (HSS tools) was 0.6-0.8 mm per tooth. For aluminum, the back rake angle is 35°, while the end relief angle is 8°-10° [32], which were incorporated in the tool geometry. The elements were generated by mapped meshing and the number of elements taken up for grid independence was 0.35 million.

Before taking up FEA, the machining parameters had to be selected for the HSS tools and the aluminum alloys. For HSS tools, the milling speeds for aluminum and its alloys are in the range of 120-150 meters per minute for a rough cut, while for a finish cut, 220-250 meters per minute [32].

Table 3   Comparison of mechanical properties of the three compositions.

Composition	Yield Strength, σ_y (MPa)	Elasticity Modulus, E (MPa)	Tangent Modulus, E_t (MPa)	Density, ρ (kg/m^3)
2G	64.43	46,710.21	225.51	2,661.2
2G2S	74.32	71,619.72	260.13	2,584.8
2G4S	81.35	81,345.86	284.71	2,559.6

Table 4   Mechanical properties of high-speed steel.

Tool Material	Young's Modulus, E (MPa)	Poisson's Ratio, μ	Density, ρ (kg/m^3)
H.S.S.	220,000	0.3	7,850

FEA approaches in machining consist of two popular routes: Eulerian and Lagrangian formulations [33]. Recently, the arbitrary Eulerian-Lagrangian formulation has popularly been used in machinability studies [34]. In the current study, the Lagrangian approach was followed. For the work material, the Johnson-Cook constitutive material model was considered. Plane 162 element was chosen. The finite element material constants for AA6061-T6 are given in Table 5 [35]. Eq. (1) shows the expression for the peripheral cutting speed V, with milling cutter rotational speed N, and pitch circle diameter D. Cutting speeds of 150 mpm and 250 mpm were selected for the studies. From Eq. (1), the peripheral angular speed values were 900 rpm and 1500 rpm respectively. In the model, the base of the work was constrained to prevent the cutter from pushing away the work. The cutter was given a 'Rigid' material model to keep the focus on the machining and chip formation in the work.

$$N = \frac{1000V}{\pi D}$$

(1)

The von Mises stress and deformation of the work material were taken as the output parameters in the FE study obtained by simulation at the two cutting speeds respectively.

In experimental studies, a DTC300 three-axis high precision vertical machining center (shown in Figure 3(b)), equipped with a twelve-tool turret, was used for the surface milling operation on the stir cast slabs of the three compositions, under dry conditions. For each composition, two specimens were taken for the two cutting speeds. The cutting speeds employed were kept the same as that used during the finite element modeling, with milling conducted at 900 rpm and 1500 rpm, respectively. A constant feed rate of 5 mm/min was employed during machining of all the compositions for both speeds, with a depth of cut of 0.1 mm. The chips generated during the machining operation were collected for characterization. The surface roughness of the milled specimens was inspected using a Taylor Hobson Talysurf surface roughness tester. The surface morphology of the milled specimens and the chips generated during milling was inspected on an Olympus BX53M optical microscope.

Table 5   Finite element material constants for AA6061-T6.

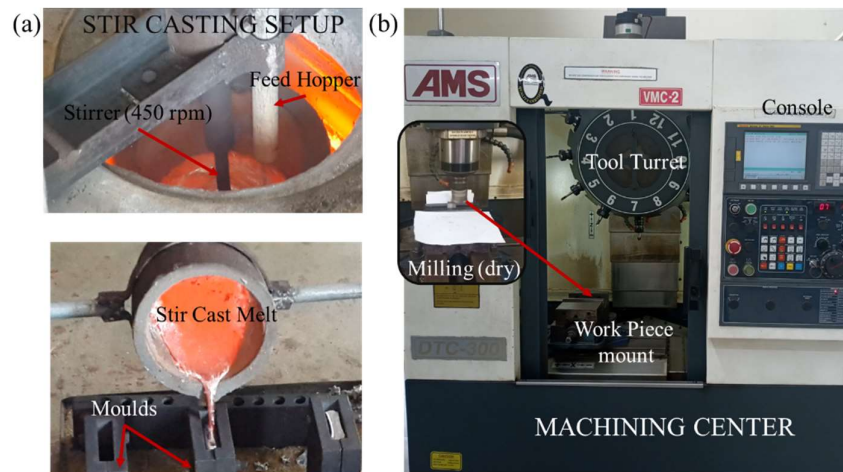| Work Material	Poisson's Ratio, μ	Strain Rate (C)	Strain Rate (P)	Hardening Parameter	Failure Strain
Aa6061-T6	0.33	6500	4	0.01	0.25

Figure 3   (a) Stir casting setup for fabrication, (b) machining center setup for face milling.

3 Results and Discussion

The results of the tensile tests for the three compositions are shown in Table 6. For ageing at 100 °C, the increase of flow stress was slower for 2G with increasing strain, moderate for 2G2S, and highest for 2G4S. This shows that work hardening took place, in the case of 2G towards the beginning of the plastic stage, while the other two compositions showed slower work hardening phenomena. The strain hardening rate decelerated with an increase in strain for 2G4S, facilitated by quicker development of dislocations and multiplications during the initial phase of plastic deformation [9].

At 180 °C, the increase of flow stress for 2G compositions was further slowed down, suggesting accelerated work hardening. 2G2S and 2G4S both display a faster increase of flow stress with strain, but this trend was sufficiently slower than that observed at 100 °C. The 2G4S composition showed the best performance in terms of yield strength and tensile strength. The yield strength for each composition was around 25% of the ultimate tensile strength. Due to the addition of reinforcements, no distinct upper or lower yield points were observed, as pure AA6061 alloy is ductile. Figure 4 shows the yield strength and the tensile strength for the three compositions. The ageing temperature of 100 ºC resulted in a higher yield strength in all compositions compared to the ageing temperature of 180 ºC. However, the ageing time was noticed to be significantly higher.

Table 6　Details of the mechanical properties obtained from the tensile tests.

Ageing Temperature	Composition	Yield Strength (MPa)	Ultimate Tensile Strength (MPa)	% Elongation
	2G	64.43	273.37	32.63%
100°C	2G2S	74.32	305.74	32.17%
	2G4S	81.35	326.55	31.73%
	2G	48.31	188.74	23.70%
180°C	2G2S	50.26	205.23	22.77%
	2G4S	55.79	237.20	19.77%

Table 7　Details of peak von Mises equivalent stress and deformation.

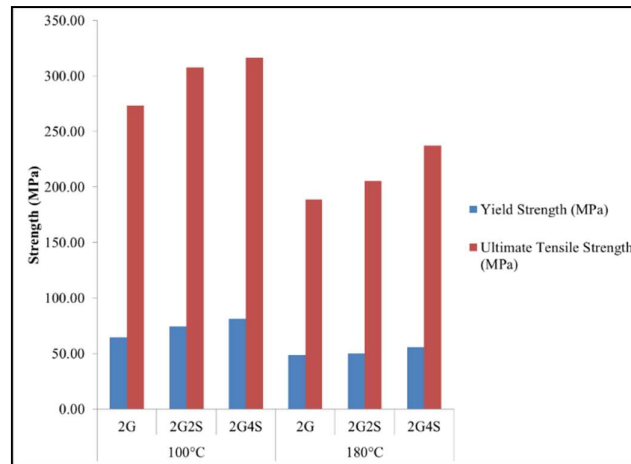| Type of Cut	Cutting Speed (rpm)	Peak von Mises Equivalent Stress (MPa)			Maximum Deformation (mm)		
		2G	2G2S	2G4S	2G	2G2S	2G4S
Low speed (Rough)	900	131.85	149.98	164.21	1.18	1.18	0.92
High speed (Rough)	1500	137.77	163.48	168.06	1.31	0.88	0.87

Figure 4 Yield strength and tensile strength for the three compositions.

Table 7 shows the variation of the von Mises equivalent stress for lower and
higher speeds for the three compositions considered in the study and the
corresponding deformations. The compositions 2G and 2G4S showed values
closer to the peak Von Mises stress for both cutting speeds, while 2G2S showed
a significant difference between the two cuts. Since the yield and elastic stresses
and the tangent modulus increased with the content of granite dust, the von Mises
stresses also showed an increasing trend, with maxima of 168.06 MPa for 2G4S.

Figures 5, 6 and 7 shows the simulation results for the 2G, 2G2S and 2G4S
compositions, respectively, at the two cutting speeds. In the 2G composition, the
deformation (mm) was found to increase with increasing speed. The presence of
the granite dust particles in the 2G2S and 2G4S compositions led to a decrease in
deformation with an increase in cutting speed. Upon increasing the weight
fraction of the granite dust, there was an enhancement in the mechanical
properties, which when coupled with the ageing treatment, augmented the
stiffness, thus lowering the respective deformations. Upon increasing the cutting
speed, instead of continuous and long chips, segmented chips are observed for
most materials [36]. At lower speed, composition 2G generated fairly continuous
chips while at higher speed, segmented chips appeared. Aluminum can undergo
extensive plastic deformation before fracture and hence controlling chips during
machining operations is a challenge. These continuous chips may get entangled
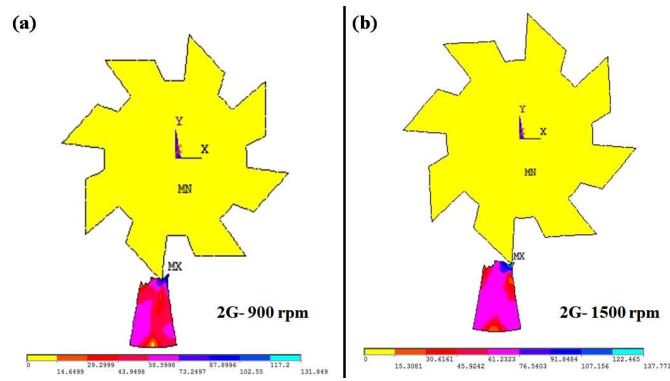with the tooling and obstruct further machining.

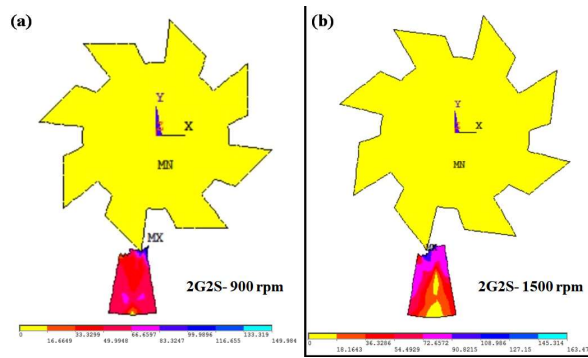**Figure 5** Machining of 2G composition at (a) 900 rpm (b) 1500 rpm.

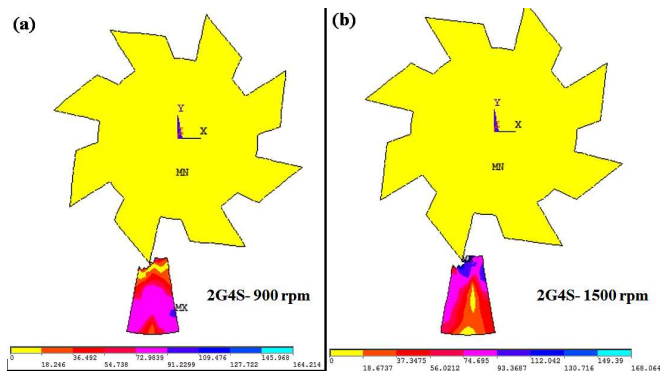**Figure 6** Machining of 2G2S composition at (a) 900 rpm (b) 1500 rpm.

Figure 7 Machining of 2G4S composition at (a) 900 rpm (b) 1500 rpm.

Figure 8 shows the effect of the two milling speeds on the surface roughness of the three compositions. For the three compositions, the surface roughness was found to decrease with the increase in milling speed, with the feed kept constant at 5 mm/min. As the weight content of the granite dust particulates increased, there was a drastic increase in the R_a value under dry milling conditions at lower speed: 35% increase for 2G2S and 165% increase for 2G4S compared to 2G. Meanwhile, at higher speed, the increase in R_a was 21.6% for 2G2S and 78.3% for 2G4S, respectively.
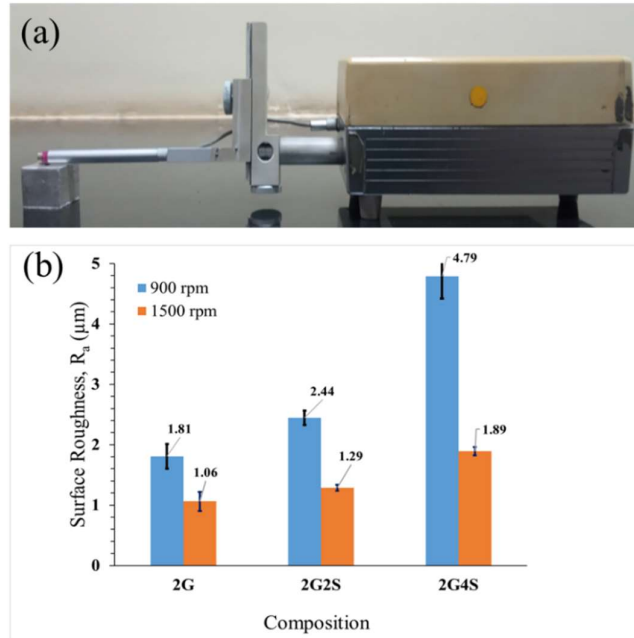

Figure 8 (a) Taylor Hobson Talysurf surface roughness tester, (b) surface roughness (R_a) variation of the milled specimens.

The optical micrographs shown in Figure 9 were used to investigate the surface textures of the three compositions after surface milling at the two cutting speeds. In 2G, the presence of lubricating graphite particulates proved beneficial during the machining since only micro plowing was observed on the surface at both speeds. In 2G2S, at both speeds, micro plowing with scratches and scoring marks due to abrasion caused by freed hard granite dust particles. The presence of graphite was beneficial to the micro plowing. In 2G4S, the higher content of hard granite dust particles was responsible for severe plowing along with galling and abrasive wear. At higher speeds, the release of the granite dust particles was faster, causing a higher degree of wear and plowing.
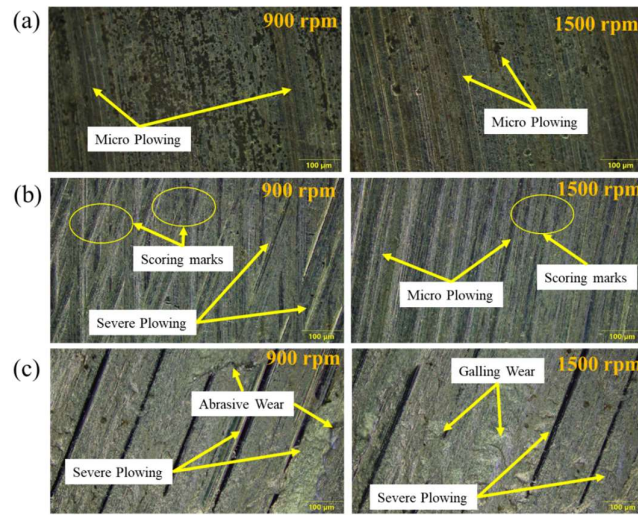
Figure 9 Surface morphology of the three compositions after face milling, (a) 2G, (b) 2G2S, (c) 2G4S.

Figure 10 shows the types of chips formed in the three compositions at the two different speeds. Longer chips with an arc shape and equidistant sawtooth folds (Figure 10(a)) were observed at both speeds for 2G as compared to the other two compositions, which is generally observed for AA6061 alloys [37,38].
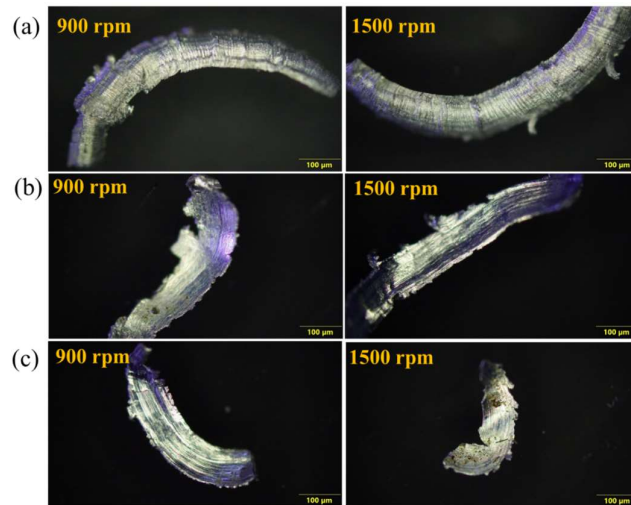

Figure 10 Chip classification and morphology, (a) 2G, (b) 2G2S, (c) 2G4S.

The 2G2S and 2G4S compositions developed segmented, discontinuous chips [36,39] during machining, irrespective of cutting speed. This can be attributed to the presence of granite dust, which promotes plastic instability and provides sites for breakage of the chips. Thus, hybrid composites of graphite and granite dust as fillers can overcome the formation of continuous chips. A similar morphology of the chips was observed while carrying out milling of the cast slabs of these three compositions.

4 Conclusion

The effect of the peripheral speeds during milling operation of hybrid AA6061 matrix composites was studied using FEM and experimental studies. The following conclusions can be drawn:

1. In all three compositions, the FE analysis showed an increase in the von Mises stress and the material deformation with an increase in the cutting speed. However, with an increase in the content of ceramic filler, the von Mises stress and the deformation were found to increase correspondingly.
2. The hybrid composites of aluminum alloys containing ceramic reinforcements led to faster wear of the milling tool at higher cutting speeds (conventionally used for aluminum alloys). To improve tool life, carbide coated HSS or carbide tools are necessary to machine the hybrid composites at high cutting speeds.
3. The surface roughness values were found to increase with an increase in ceramic content. The surface finish of the 2G composition showed that the presence of graphite aids the machinability as it imparts dry lubrication at the cutting zones, lowering the friction between the tool and the chip interface, with surface texture displaying micro plowing.
4. From the surface texture analysis, increasing the content of granite dust particles led to severe plowing and abrasive wear, with the effects more pronounced at higher speed.
5. By adding ceramic reinforcements, the age-old challenge of long, strain hardened continuous chips during machining of aluminum and its alloys could be overcome, with discontinuous, segmented chips being formed.
6. The addition of ceramic reinforcement leads to a drop in the plasticity of AA6061 alloys, as is evident from the transition from long, continuous chips in 2G to discontinuous, segmented chips in 2G2S and 2G4S.

References

[1]   Gay, D., Hoa, S.V. & Tsai, S.W., *Composite Materials Science and Applications*, CRC Press, 2003.

[2]   Narayanasamy, R., Srinivasan, M. & Loganathan, C., *Characteristics of Al 6061 / TiO 2p / Al 2 O 3p*, Metal Matrix Composites, **1**(6), pp. 75-78, 2008

[3]   Bodukuri, A. K., Eswaraiah, K., Rajendar, K. & Sampath, V*., Fabrication of Al–Sic–B4C Metal Matrix Composite by Powder Metallurgy Technique and Evaluating Mechanical Properties*, Perspectives in Science **8**, pp. 428-431, 2016.

[4]   Deaquino-Lara, R., Gutiérrez-Castañeda, E., Estrada-Guel, I., Hinojosa-Ruiz, G., García-Sánchez, E., Herrera-Ramírez, J.M., Pérez-Bustamante, R. & Martínez-Sánchez, R., *Structural Characterization of Aluminium Alloy 7075-Graphite Composites Fabricated by Mechanical Alloying and Hot Extrusion*, Materials and Design, **53**, pp. 1104-1111, 2014.

[5]   Su, J., Wu, G.H., Li, Y., Gou, H. S., Chen, G.H. & Xiu, Z. Y., *Effects of Anomalies on Fracture Processes of Graphite Fiber Reinforced Aluminum Composite*, Materials and Design, **32**(3), pp. 1582-1589, 2011.

[6]   Suresha, S. & Sridhara, B. K., *Effect of Addition of Graphite Particulates on The Wear Behaviour in Aluminium-Silicon Carbide-Graphite Composites*, Materials and Design, **31**(4), pp. 1804-1812, 2010.

[7]   Guo, M.L.T. & Tsao, C.Y.A., *Tribological Behavior of Self-Lubricating Aluminium/Sic/Graphite Hybrid Composites Synthesized by The Semi-Solid Powder-Densification Method*, Composites Science and Technology, **60**(1), pp. 65-74, 2000.

[8]   Chu, H. Y. & Lin, J. F., *Experimental Analysis of the Tribological Behavior of Electroless Nickel-Coated Graphite Particles in Aluminum Matrix Composites under Reciprocating Motion*, Wear, **239**(1), pp. 126-142, 2000.

[9]   Alidokht, S.A., Abdollah-zadeh, A., Soleymani, S. & Assadi, H., *Microstructure and Tribological Performance of an Aluminium Alloy Based Hybrid Composite Produced By Friction Stir Processing*, Materials and Design, **32**(5), pp. 2727-2733, 2011.

[10]   Baradeswaran, A. & Perumal, A.E., *Wear and Mechanical Characteristics of Al 7075/graphite Composites*, Composites Part B: Engineering, 56, pp. 472-476, 2014.

[11]   Poovazhagan, L., Kalaichelvan, K., Rajadurai, A. & Senthilvelan, V., *Characterization of Hybrid Silicon Carbide and Boron Carbide Nanoparticles-Reinforced Aluminum Alloy Composites*, Procedia Engineering, **64**, pp. 681-689, 2013.

[12]   Alaneme, K.K., Akintunde, I.B., Olubambi, P.A. & Adewale, T.M., *Fabrication Characteristics And Mechanical Behaviour of Rice Husk Ash - Alumina Reinforced Al-Mg-Si Alloy Matrix Hybrid Composites*, Journal of Materials Research and Technology, **2**(1), pp. 60-67, 2013.

[13]   Ahamed, H. & Senthilkumar, V., *Experimental Investigation on Newly Developed Ultrafine-Grained Aluminium Based Nano-Composites with Improved Mechanical Properties*, Materials and Design, **37**, pp. 182–192, 2012.

[14]   Rajan, T.P.D., Pillai, R.M., Pai, B.C., Satyanarayana, K.G. & Rohatgi, P.K., *Fabrication And Characterisation Of Al-7Si-0.35Mg/Fly Ash Metal Matrix Composites Processed By Different Stir Casting Routes*, Composites Science and Technology, **67**(15–16), pp. 3369–3377, 2007.

[15]   Narasimha Murthy, I., Venkata Rao, D. & Babu Rao, J., *Microstructure and Mechanical Properties of Aluminum-Fly Ash Nano Composites Made by Ultrasonic Method*, Materials and Design, **35**, pp. 55-65, 2012.

[16]   Sudarshan, Surappa, M.K., *Dry Sliding Wear of Fly Ash Particle Reinforced A356 Al Composites*, Wear, **265**(3-4), pp. 349-360, 2008.

[17]   Ozturk, F., Sisman, A., Toros, S., Kilic, S. & Picu, R. C., *Influence of Aging Treatment on Mechanical Properties of 6061 Aluminum Alloy*, Materials and Design, **31**(2), pp. 972–975, 2010.

[18]   Adesola, A.O., Odeshi, A.G. & Lanke, U.D., *The Effects of Aging Treatment and Strain Rates on Damage Evolution in AA 6061 Aluminum Alloy in Compression,* Materials and Design, **45**, pp. 212–221, 2013.

[19]   Rajasekaran, S., Udayashankar, N. K. & Nayak, J., *T4 and T6 Treatment of 6061 Al-15 Vol.% SiC P Composite,* ISRN Materials Science, 2012, pp. 1-5, 2012.

[20]   Pai, A., Sharma, S.S., D'Silva, R. E. & Nikhil, R.G., *Effect of Graphite and Granite Dust Particulates as Micro-Fillers on Tribological Performance of Al 6061-T6 Hybrid Composites*, Tribology International, **92**, pp. 462-471, 2015.

[21]   Sharma, S.S., Pai, A. & Gowrishankar, M.C., *Potentiality of Artificially Aged Aluminium 6061 Hybrid Composites Reinforced with Granite and Graphite Micro–Fillers for Structural Applications: Potenzial Von Künstlich Gealterten, Mit Granit Und Graphit Verstärkten Aluminium-(6061) Hybrid-Verbundwerks*, Materialwissenschaft und Werkstofftechnik, **48**(11), pp. 1082-1092, 2017.

[22]   Sayuti, M., Sarhan, A.A.D. & Hamdi, M., *An investigation of Optimum Sio2 Nanolubrication Parameters in end Milling of Aerospace Al6061-T6 Alloy*, International Journal of Advanced Manufacturing Technology, **67**(1-4), pp. 833-849, 2013.

[23]   Jin, X. & Altintas, Y., *Prediction of Micro-Milling Forces with Finite Element Method*, Journal of Materials Processing Technology, **212**(3), pp. 542-552, 2012.

[24] Rai, J.K. & Xirouchakis, P., *Finite Element Method Based Machining Simulation Environment for Analyzing Part Errors Induced During Milling of Thin-Walled Components*, International Journal of Machine Tools and Manufacture, **48**(6), pp. 629-643, 2008.

[25] Ghafarizadeh, S., Chatelain, J. F. & Lebrun, G., *Finite Element Analysis of Surface Milling of Carbon Fiber-Reinforced Composites*, International Journal of Advanced Manufacturing Technology, **87**(1-4), pp. 399-409, 2016.

[26] Mebrahitom, A., Choon, W. & Azhari, A., *Side Milling Machining Simulation Using Finite Element Analysis: Prediction of Cutting Forces*, Materials Today: Proceedings, **4**(4), pp. 5215-5221, 2017.

[27] Krajinović, I., Daves, W., Tkadletz, M., Teppernegg, T., Klünsner, T., Schalk, N., Mitterer, C., Tritremmel, C., Ecker, W. & Czettl, C., *Finite Element Study of The Influence of Hard Coatings on Hard Metal Tool Loading During Milling*, Surface and Coatings Technology, **304**, pp. 134-141, 2016.

[28] Yang, D., Liu, Z., Ren, X. & Zhuang, P., *Hybrid Modeling with Finite Element and Statistical Methods for Residual Stress Prediction in Peripheral Milling of Titanium Alloy Ti-6Al-4V*, International Journal of Mechanical Sciences, **108-109**, pp. 29-38, 2016.

[29] Davoudinejad, A., Tosello, G., Parenti, P. & Annoni, M., *3D Finite Element Simulation of Micro End-Milling by Considering the Effect of Tool Run-out*, Micromachines, **8**(6), pp. 1-20, 2017.

[30] Davoudinejad, A., Tosello, G. & Annoni, M., *Influence of the Worn Tool Affected by Built-Up Edge (BUE) on Micro End-Milling Process Performance: A 3D Finite Element Modeling Investigation*, International Journal of Precision Engineering and Manufacturing, **18**(10), pp. 1321-1332, 2017.

[31] Ucun, İ., Aslantas, K. & Bedir, F., *Finite Element Modeling of Micro-Milling: Numerical Simulation and Experimental Validation*, Machining Science and Technology, **20**(1), pp. 148-172, 2016.

[32] Walsh, R.A. Handbook of machining and metalworking calculations. 2001

[33] Benson, D.J. & Okazawa, S., Contact in a Multi-Material Eulerian Finite Element Formulation, Computer methods in Applied Mechanics and Engineering, **193**(39-41), pp. 4277–4298, 2004.

[34] Llanos, I., Villar, J.A., Urresti, I. & Arrazola, P.J., *Finite Element Modeling of Oblique Machining using an Arbitrary Lagrangian–Eulerian formulation*, Machining Science and Technology, **13**(3), pp. 385-406, 2009.

[35] Urankar, S., Lovell, M., Morrow, C., Li, Q. & Kawada, K., *Development of a Critical Friction Model for Cross Wedge Rolling Hollow Shafts,* Journal of Materials Processing Technology, **177**(1-3), pp. 539-544, 2006.

[36] Childs, T., Maekawa, K., Obikawa, T. & Yamane, Y., *Metal Machining: Theory and Application*, 2000. DOI:10.1016/c2009-0-23990-0.

[37] Pan, J., Ni, J., He, L., Cui, Z. & Feng, K., *Influence of Micro-Structured Milling Cutter on The Milling Load and Surface Roughness of 6061 Aluminum Alloy*, International Journal of Advanced Manufacturing Technology **110**(11-12), pp. 3201-3208, 2020.

[38] Liu, Y., Gong, Y., Liu, W., Sun, X. & Xu, L., *Effect of milling parameters on Chip Shape and Chip Morphology for Zr-Based Bulk Metallic Glass by Using Micro-Groove Milling*, International Journal of Advanced Manufacturing Technology **111**(5-6), pp. 1587-1602, 2020.

[39] Ebersbach, F.G., Builes, S.D., Dorneles, C.F., Schroeter, R.B., Binder, C., Klein, A.N. & de Mello, J.D.B., *Effect of Cutting Parameters in Machining Force, Surface Texture and Chipsmorphology Obtained in Turning of Sintered Self-Lubricating Composites*, Materials Research, **23**(4), pp. 1-10, 2020.